Optical Engineering

OpticalEngineering.SPIEDigitalLibrary.org

Image contrast model of non-line-of-sight imaging based on laser range-gated imaging

Kaida Xu
Weiqi Jin
Shenyou Zhao
Jing Liu
Hui Guo
Su Qiu
Dongsheng Wu

SPIE.

Image contrast model of non-line-of-sight imaging based on laser range-gated imaging

Kaida Xu,[a] Weiqi Jin,[a,b] Shenyou Zhao,[a] Jing Liu,[a] Hui Guo,[b] Su Qiu,[a,b] and Dongsheng Wu[a]
[a]Beijing Institute of Technology, School of Optoelectronics, Ministry of Education Key Laboratory of Photoelectronic Imaging Technology and System, Beijing, 100081, China
[b]National Key Laboratory of Science and Technology on Low Light Level Night Vision, Shan Xi, Xi'an 710065, China

Abstract. Laser range-gated imaging systems can obtain images of targets hidden around the corner, with an intermediary reflective surface with certain specular reflection characteristics. This imaging mode is called non-line-of-sight imaging. This paper describes a simulation of the target signal illuminance and disturbance radiation on the photosensitive surface of a non-line-of-sight imaging system based on modeling of an intermediary reflective surface. Meanwhile, an image contrast model of a non-line-of-sight imaging system is constructed. Simulation of the image contrast for a laser range-gated imaging system as a non-line-of-sight imaging equipment was carried out by analyzing the effects of varying the target signal illuminance and intermediary reflective surface reflection. Our simulation results show that the reflection characteristics of the intermediary reflective surface have a significant effect on the non-line-of-sight imaging. Although ordinary active laser imaging can realize non-line-of-sight imaging for an intermediary reflective surface with significant specular reflection characteristics, a laser range-gated imaging system is indispensable for non-line-of-sight imaging with commonly used intermediary reflective surfaces without significant specular reflection characteristics. The image contrast model of non-line-of-sight imaging constructed in this paper provides insights into the theoretical analysis and system design, as well as practical application of non-line-of-sight imaging. [DOI: 10.1117/1.OE.53.6.061610]

Keywords: range-gated imaging; non-line-of-sight imaging; laser imaging; image contrast model; intermediary reflective surface.

Paper 131353SS received Sep. 1, 2013; revised manuscript received Nov. 11, 2013; accepted for publication Nov. 12, 2013; published online Dec. 16, 2013; corrected Dec. 18, 2013.

1 Introduction

Laser range-gated imaging can penetrate a strong scattering medium and capture the image of an object at a certain distance by applying active laser illumination, changing the gate delay time, and varying the gate width. It has been widely used in areas such as military reconnaissance, monitoring, underwater detection, and search and rescue. For cases when the line of sight is blocked by corners of walls or other building obstructions within the environment of city streets and buildings (as shown in Fig. 1), traditional imaging techniques and equipment are unable to achieve imaging beyond the direct field of view. Non-line-of-sight imaging can bypass the corners of walls or other obstructions to achieve imaging beyond the direct field of view, which can be used to reduce casualties in modern urban street fighting, and to increase battlefield awareness and operational efficiency.

In 2006 and 2007, researchers at the Research Institute for Optronics and Pattern Recognition of Germany and Swedish Defence Research Agency (FOI)[1,2] of Sweden carried out joint research on short-wavelength infrared laser range-gated imaging for ground applications in monostatic and bistatic configurations. A number of test targets (test panels, vehicles, and soldiers with weapons) were included in the tests, and windows in buildings and cars, traffic signs, and vehicle surfaces were utilized as the intermediary reflective surfaces. In 2011, the FOI group[3] proposed the loss factor model through further study of the effect of the characteristics (including the shape and the reflection characteristics) of the intermediary reflective surface on laser illuminance attenuation and measured the loss factors with different intermediary reflective surfaces. Though their work was insightful, their model is not effective for describing the imaging process. Since 2007, the Media Lab at the Massachusetts Institute of Technology (MIT)[4] has been studying transient imaging based on femtosecond laser range-gated imaging technology and proposed an algorithm for extracting object information from multireflection, realizing a means of seeing around the corner. In 2012, researchers at MIT[5] realized a three-dimensional reconstruction of hidden targets utilizing diffuse reflections of ultrashort laser pulses using an intermediary reflective surface. Since 2012, researchers at the Beijing Institute of Technology (BIT)[6,7] have been studying non-line-of-sight imaging. The BIT group uses a nanosecond laser range-gated imaging system to realize non-line-of-sight imaging of an USAF 1951 standard target at different distances with glass and ceramic tile as the respective intermediary reflective surfaces. These existing researches show the potential application prospects of non-line-of-sight imaging in areas such as urban warfare, counter-terrorism, and disaster relief.

Since non-line-of-sight imaging based on laser range-gated imaging is affected not only by the parameters of the laser range-gated imaging system but also by the reflection characteristics of the intermediary reflective surface and the scene, construction of an optical imaging model is important to the development and application of non-line-of-sight

Address all correspondence to: Kaida Xu, Beijing Institute of Technology, 5 South Zhongguancun, Street, Haidian District, Beijing, 100081. Tel: 86-10-68914697; Fax: 86-10-68912569-816; E-mail: jinwq@bit.edu.cn

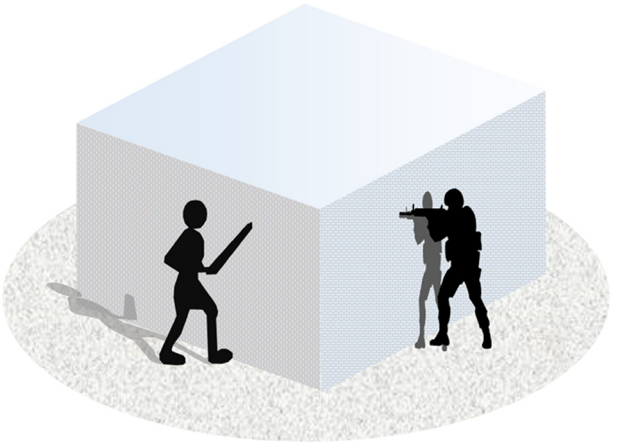

Fig. 1 Representation of the line of sight being blocked by the corner of a structure.

imaging. This paper describes the construction of an image contrast model of non-line-of-sight imaging from the viewpoint of a two-dimensional illumination distribution on the photosensitive surface, in order to analyze the performance of a non-line-of-sight imaging system utilizing a laser range-gated imaging system and to provide a theoretical basis for actual non-line-of-sight imaging system design.

2 Principle of Non-Line-of-Sight Imaging

The key to non-line-of-sight imaging is to make it possible to see a street-corner target or an indoor target by utilizing an intermediary reflective surface, as illustrated in Fig. 2. A is the observer, B is the target under observation, and C is the intermediary reflective surface. B is outside the range of objects that can be directly imaged by A, so that C is utilized to realize non-line-of-sight imaging of target B.

A laser range-gated imaging system, consisting of a nanosecond laser and an intensified charged coupled device (ICCD) imaging system, is located at location A. The ICCD imaging system is focused on location B. The beam from the nanosecond laser from location A experiences first-order reflections (consisting of first-order specular reflection and first-order diffuse reflections, where the first-order diffuse reflection contains first-order backscattering and first-order forward-scattering) at the intermediary reflective surface C. The first-order specular reflection and first-order forward-scattering illuminate target B and then are reflected at target

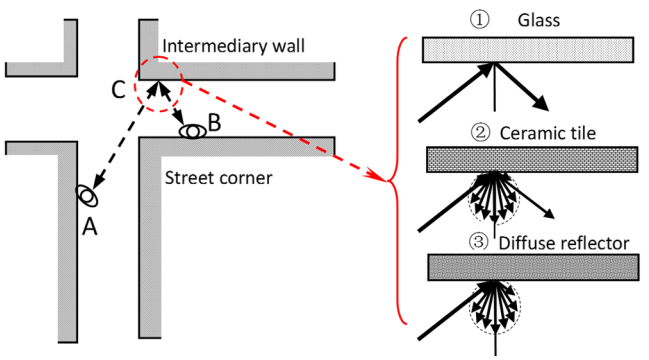

Fig. 2 Non-line-of-sight imaging and modeling of the intermediary reflective surfaces.

B in a Lambertian fashion (the second-order reflection). First-order backscattering is received by the ICCD imaging system, forming a defocused image and reducing the image contrast of target B. The second-order Lambertian reflection strikes the intermediary reflective surface C and experiences third-order reflections (consisting of third-order specular reflection, third-order backscattering, and third-order forward-scattering) at location C. Third-order specular reflection is received by the ICCD imaging system, forming a focused image of target B. Like the first-order backscattering, the third-order forward-scattering is also received by the ICCD imaging system, reducing the contrast of the image of target B.

For certain intermediary reflective surfaces (like ceramic tile), the effective target signal illuminance (third-order specular reflection) may be overwhelmed by the first-order backscattering and third-order forward-scattering, resulting in the target being undetectable. The first-order backscattering is apparently larger than the third-order forward-scattering, so the first-order backscattering is the dominant factor reducing the contrast of the image of target B. Thus, a better non-line-of-sight image of target B can be obtained by filtering out the first-order backscattering, which can be realized by laser range-gated imaging. Meanwhile, an image intensifying technique is also needed because the effective target signal illuminance (third-order specular reflection) is typically weak. The intermediary reflective surface is also a very important factor in non-line-of-sight imaging, which can be generalized to include a full specular reflector like glass (1), a partial specular reflector like ceramic tile (2), and an ideal diffuse surface (3). The study in this paper is mainly carried out on intermediary reflective surface types 1 and 2.

Construction of an optical imaging model of the non-line-of-sight imaging process, which is based on the parameters of the intermediary reflective surface, the parameters of the laser range-gated imaging system, and the properties of the target, is vital for the theoretical analysis and system design of non-line-of-sight imaging based on laser range-gated imaging. This model assumes that the imaging will occur at night or in low-light conditions to reduce the impact of environmental illuminance.

3 Image Contrast Model of Non-Line-of-Sight Imaging

As shown in Fig. 3, the laser beam is projected onto an intermediary reflective surface forming the light spot S_1 and experiences first-order reflections; then the first-order reflections are projected onto the target forming light spot S_2. The distance from the laser to the geometric center of S_1 is l_1. The distance from the geometric center of S_1 to the geometric center of S_2 is l_2. The vector tracing the direction of the incident light from S_1 to S_2 makes an angle α with $\mathbf{n}_1$ (the vector normal to S_1) and an angle β with $\mathbf{n}_2$ (the vector normal to S_2). The optical axis of the laser and the optical axis of the ICCD are assumed to be coincident, and the divergence angle of the laser and the field view angle of the ICCD are also assumed to be coincident. In this section, the laser transmission characteristics (attenuation and distribution) in the non-line-of-sight imaging process will be analyzed.

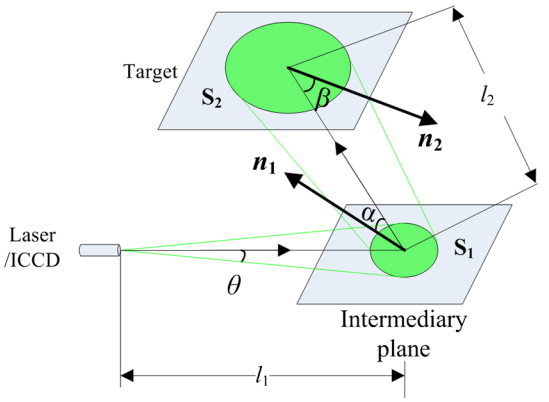

Fig. 3 Diagram of laser propagation.

3.1 *Pulsed Laser and Range-Gated Imaging System*

$$I_0(t) = \frac{P(t)}{\Omega_{\text{laser}}} = \frac{\Phi}{t_p \cdot \Omega_{\text{laser}}} \cdot \text{rect}\left[\frac{1}{t_p}\left(t + \frac{t_p}{2}\right)\right] = I_0 \cdot \text{rect}\left[\frac{1}{t_p}\left(t + \frac{t_p}{2}\right)\right], \tag{1}$$

$$\Omega_{\text{laser}} = \pi \sin^2 \theta, \tag{2}$$

$$\text{rect}(t) = \begin{cases} 0 & |t| > 1/2 \\ 1/2 & |t| = 1/2 \\ 1 & |t| < 1/2 \end{cases}. \tag{3}$$

The illuminance of the pulsed laser can be written as shown in Eq. (1), where $P(t)$ denotes the transmission power of the pulsed laser, t is the propagation time, Φ is the energy of a single pulse, t_p is the pulse width, Ω_{laser} is the solid angle of the divergence of the laser beam, and θ is half divergence angle of the laser beam. The function $\text{rect}(t)$ is described by Eq. (3). The detector includes $M \times N$ pixels, t_g is the gate width, and t_d is the strobe gating delay time.

3.2 *Reflection Characteristics of the Intermediary Reflective Surface*

The reflection characteristics (consisting of specular reflection characteristics and diffuse reflection characteristics) of the intermediary reflective surface are among the important factors that can influence the non-line-of-sight imaging results. Without loss of generality, the intermediary reflective surface is assumed to be free of absorption, so that its reflection characteristics can be described by the specular reflectivity ρ_s and the diffuse reflectivity ρ_d. ρ_s is a constant, ρ_d obeys Lambertian reflection, and $\rho_s = 1 - \rho_d$. The reflectance distribution function is described by

$$\rho(\theta, \varphi, \theta_i) = \frac{\rho_d}{2\pi} \cos(\theta) + (1 - \rho_d)\delta(\theta + \theta_i, \varphi + \pi), \tag{4}$$

with

$$\int_0^{2\pi} \int_0^{\pi/2} \rho(\theta, \varphi, \theta_i) \mathrm{d}\varphi \mathrm{d}\theta = 1. \tag{5}$$

3.3 *Target Signal Illuminance and Disturbance Caused by the Intermediary Reflective Surface under CW-Laser Illumination*

3.3.1 *Illuminance on the target plane S_2*

The illuminance on the target plane S_2 is denoted as E_2, which consists of two parts: E_{2s} is caused by the first-order specular reflection of the laser and E_{2d} is caused by the first-order forward-scattering. The illuminance on S_1 should be obtained first.

Illuminance on S_1. According to Eq. (1), the illuminance on S_1 is given by

$$E_1 = \frac{I_0 \cdot \cos \alpha}{l_1^2} = \frac{\Phi \cdot \cos \alpha}{t_p \cdot \Omega_{\text{laser}} \cdot l_1^2}. \tag{6}$$

First-order specular reflection. The area illuminated on S_2 by the laser first-order specularly reflected by S_1 can be written as

$$s_2 = \frac{(l_1 + l_2)^2 \cdot \Omega_{\text{laser}}}{\cos \beta}. \tag{7}$$

Therefore, E_{2s} can be calculated as

$$E_{2s} = \frac{P \cdot \rho_s}{s_2} = \frac{P \cdot \rho_s}{(l_1 + l_2)^2 \cdot \Omega_{\text{laser}}} \cdot \cos \beta. \tag{8}$$

The target distance l is equal to the sum of l_1 and l_2. If l is much larger than the square root of s_2, and S_2 is illuminated by the vertically incident laser beam ($\cos \beta = 1$), Eq. (8) can be further simplified.

First-order forward-scattering. To facilitate the analysis and calculations, Fig. 3 is expanded along the optical path. Assuming that the optical axis of the laser coincides with the optical axis of the ICCD imaging system, a Cartesian coordinate system is established with the geometric center of the lens as the Cartesian coordinate origin. The optical axis is along the z axis, and the y axis and the x axis are, respectively, parallel to the detector array's length and width directions, as is shown in Fig. 4. φ is the angle between the x axis and the projection of $\mathbf{n}_1$ on the xoy plane, and $\mathbf{n}_2$ points in the direction opposite to the direction of the z axis. S_1 and S_2 are, respectively, projections of the laser beam on the intermediary reflective surface and on the target.

According to the geometric relationship, the projection equations for S_1 and S_2 on the xoy plane are, respectively, given by

$$x^2 + y^2 - \text{tg}^2\theta \cdot [\text{tg}\alpha \cdot (x \cos \varphi - y \sin \varphi) + l_1]^2 \le 0, \tag{9}$$

$$x^2 + y^2 - \text{tg}^2\theta \cdot (l_1 + l_2)^2 \le 0. \tag{10}$$

$P_1(x_1, y_1, z_1)$ and $P_2(x_2, y_2, z_2)$ are random points, respectively, on S_1 and S_2, and d_{S1} is a microsurface element around $P_1(x_1, y_1, z_1)$ (as shown in Fig. 5).

$$dE_{2d} = \frac{L_1 \cdot ds_1}{l_{p2}^2} \cdot \cos\gamma_2 \cdot \cos\eta_2 = \frac{E_1 \cdot \rho_d \cdot \cos\eta_2 \cdot \cos\gamma_2}{\pi \cdot l_{p2}^2 \cdot \cos\alpha} \mathrm{d}x_1 \mathrm{d}y_1. \tag{11}$$

dE_{2d} is the illuminance on $P_2(x_2, y_2, z_2)$ caused by d_{S1}. The illuminance is inversely proportional to the square of the distance as in Eq. (11), where γ_2 is the angle between vectors $\overrightarrow{P_1P_2}$ and $\mathbf{n}_1$ and η_2 is the angle between vectors $\overrightarrow{P_1P_2}$ and $\mathbf{n}_2 = (0, 0, -1)$.

$$\cos\gamma_2 = \frac{\mathrm{tg}\alpha\cos\varphi(x_2 - x_1) + \mathrm{tg}\,\alpha\cos\varphi(y_2 - y_1) - (z_2 - z_1)}{\sqrt{(x_2 - x_1)^2 + (y_2 - y_1)^2 + (z_2 - z_1)^2}\sqrt{1 + \mathrm{tg}^2\alpha}} \quad \left(0 \le \gamma_2 \le \frac{\pi}{2}\right), \tag{12}$$

$$\cos\eta_2 = \frac{-(z_2 - z_1)}{\sqrt{(x_2 - x_1)^2 + (y_2 - y_1)^2 + (z_2 - z_1)^2}} \quad \left(0 \le \eta_2 \le \frac{\pi}{2}\right), \tag{13}$$

$$l_{p2}^2 = (x_2 - x_1)^2 + (y_2 - y_1)^2 + (z_2 - z_1)^2. \tag{14}$$

Therefore,

$$E_{2d} = \iint_{S_1} dE_{2d} \qquad \left(\alpha + \theta < \frac{\pi}{2}\right). \tag{15}$$

In summary,

$$E_2 = E_{2s} + E_{2d}. \tag{16}$$

3.3.2 *Target signal illuminance on the photosensitive surface*

$$E_{su} = \frac{1}{4} \cdot \pi \cdot L_u \cdot \tau_o \cdot \rho_s \cdot \left(\frac{D_0}{f'}\right)^2 \Big/ \left[1 + \frac{1}{4} \cdot \left(\frac{D_0}{f'}\right)^2\right] = \frac{\pi \cdot L_u \cdot \tau_o \cdot \rho_s}{1 + 4F^2}. \tag{17}$$

Assuming that the target plane and the photosensitive surface of the laser range-gated imaging system are conjugate object plane and image plane, and that l is much larger than $f'(l \gg f')$, the illuminance on the photosensitive surface caused by the scene can be expressed as Eq. (17), where $L_u = \rho_u E_2/\pi$ is the luminance on S_2 (ρ_u is the reflectance of the target or background, for $u = t$ or b), $F = f'/D_0$ denotes the F-number, D_0 is the aperture diameter, and τ_o is the spectral transmittance of the objective lens.

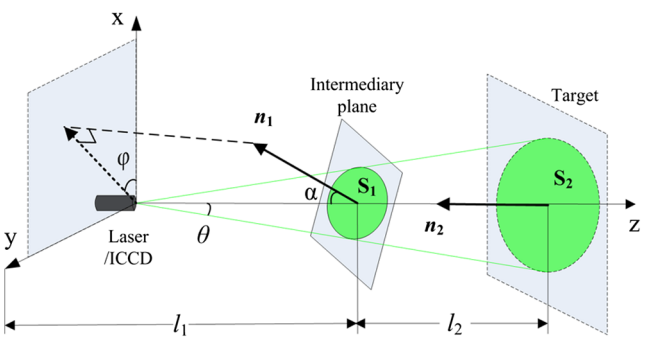

Fig. 4 Diagram illustrating the propagation of the laser beam expanded along the optical path.

3.3.3 *Disturbance illuminance on the photosensitive surface caused by scattering of the intermediary reflective surface*

The disturbance illuminance on the photosensitive surface caused by scattering of the intermediary reflective surface consists of two parts: E_d (third-order forward-scattering) and E_{back} (first-order backscattering). Since the intermediary reflective surface is not on the target plane, each point on S_1 corresponds to a diffuse plaque on the photosensitive surface, and the diffuse plaque can be expressed by a point spread function. A Cartesian coordinate system is established with the geometric center of the lens as a Cartesian coordinate origin. $P(0, 0, l_1)$ is the intersection of the intermediary reflective surface and the z axis, and P' is the image point of P, as shown in Fig. 6.

According to geometrical optics, the center of the diffuse plaque for point (x_1, y_1) on S_1 is given by

$$(x_0', y_0') = (-nl'x_1/l_1, -nl'y_1/l_1), \tag{18}$$

where

$$l' = \frac{l \cdot f'}{l - n \cdot f'}. \tag{19}$$

The radius of the diffuse plaque can be written as

$$r_0(z) = \frac{1}{2}\left\{\left[1 - \frac{(z - n \cdot f') \cdot l'}{zf'}\right] \cdot D_0\right\} = \frac{1}{2}\left\{\left[1 - \frac{(l_1 + \mathrm{tg}\alpha \cdot x_1 - n \cdot f') \cdot l'}{(l_1 + \mathrm{tg}\alpha \cdot x_1)f'}\right] \cdot D_0\right\}, \tag{20}$$

where D_0 is the aperture diameter and $n = 1$ is the refractive index of the object space.

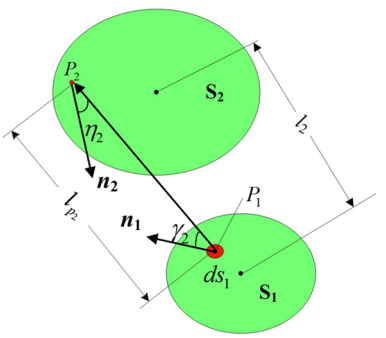

Fig. 5 Diagram of the microsurface element source.

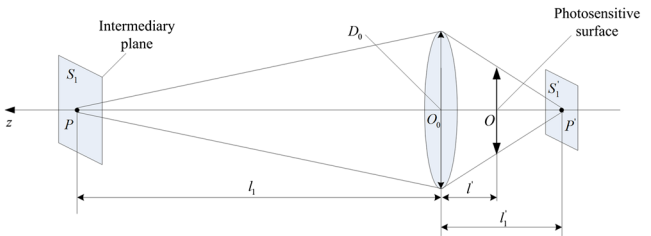

Fig. 6 Imaging relation of a point on the intermediary plane.

The point spread function of the diffuse plaque for point (x_1, y_1) can be expressed as

$$h(x',y',x_1,y_1,l_1)=\operatorname{circ}\left[\frac{\sqrt{(x'-x_0')^2+(y'-y_0')^2}}{r_0(z)}\right], \tag{21}$$

with

$$\operatorname{circ}(r)=\operatorname{circ}\left(\sqrt{x^2+y^2}\right)=\begin{cases}1 & \sqrt{x^2+y^2}\le 1\\ 0 & \text{otherwise}\end{cases}. \tag{22}$$

First-order backscattering illuminance on the photosensitive surface. According to Eq. (21), the first-order backscattering E_{back} can be expressed as

$$E_{\text{back}}=\frac{E_1\cdot\rho_d\cdot\tau_o\cdot\Omega_p\cos\alpha}{\pi^2}\cdot\iint_{S_1}\frac{1}{r_0^2(z)}\operatorname{circ}\left[\frac{\sqrt{(x'-x_0)^2+(y'-y_0)^2}}{r_0(z)}\right]\mathrm{d}s_1, \tag{23}$$

with

$$\Omega_p=\pi D_0^2/4(l_1+x_1\cdot\tan\alpha)^2. \tag{24}$$

Ω_p is the solid angle defined by the rays emanating from point $P_1(x_1, y_1, z_1)$ to the aperture defined by the lens. In fact, since the distances between the camera and every point on S_1 are not the same, the value of Ω_p for each of the points is not the same. As the laser divergence angle θ is very small, an approximate treatment for Ω_p is made here.

Third-order forward-scattering illuminance on the photosensitive surface.

$$dE_1'=\frac{L_2\cdot ds_2}{l_{p_1}^2}\cdot\cos\eta_1\cdot\cos\gamma_1=\frac{E_2\cdot\rho_{\max}\cdot\cos\eta_1\cdot\cos\gamma_1}{\pi\cdot l_{p_1}^2}\mathrm{d}x_2\mathrm{d}y_2. \tag{25}$$

In Fig. 5, d_{S2} is a microsurface element around $P_2(x_2, y_2, z_2)$. dE_1' is the illuminance on $P_2(x_2, y_2, z_2)$ caused by d_{S2}. The illuminance is inversely proportional to the square of the distance as expressed in Eq. (25), where γ_1 is the angle between vectors $\overrightarrow{P_1P_2}$ and $\mathbf{n}_1$ and η_1 is the angle between vectors $\overrightarrow{P_1P_2}$ and $\mathbf{n}_2$. Then we obtain

$$E_1'=\iint_{S_2}dE_1' \qquad (\alpha+\theta<\pi/2). \tag{26}$$

Since I_p can be calculated as

$$I_p(x,y,z)=L_p\cdot\cos\alpha\cdot ds_1'=E_1'\cdot\rho_d\cdot\cos\alpha\cdot ds_1'/\pi, \tag{27}$$

the illuminance on the photosensitive surface caused by $P_1(x_1, y_1, z_1)$ can be written as

$$dE_d=\frac{E_1'\cdot\rho_d\cdot\tau_o\cdot\Omega_p\cdot\cos\alpha}{\pi^2\cdot r_0^2(z)}ds_1'. \tag{28}$$

In summary,

$$E_d=\iint_{S_1}h(x',y',x_1,y_1,l_1)\cdot dE_d. \tag{29}$$

3.4 *Image Contrast Model of Non-Line-of-Sight Imaging*

Non-line-of-sight imaging can be achieved with laser range-gated imaging with a pulsed laser; therefore it is necessary to make a distinction between third-order reflection and first-order backscattering.

3.4.1 *Illuminance on the photosensitive surface under pulsed laser illumination*

Under pulsed laser illumination, the illuminance on the photosensitive surface caused by a single pulse is a function of time t.

$$E_{su}(t)=E_{su}\cdot\operatorname{rect}\left\{\frac{1}{t_p}\left[t+\frac{t_p}{2}-\frac{2(l_1+l_2)}{c}\right]\right\} \qquad (u=t,b), \tag{30}$$

$$E_{\text{back}}(t)=E_{\text{back}}\cdot\operatorname{rect}\left[\frac{1}{t_p}\left(t+\frac{t_p}{2}-\frac{2l_1}{c}\right)\right], \tag{31}$$

$$E_d(t)=E_d\cdot\operatorname{rect}\left\{\frac{1}{t_p}\left[t+\frac{t_p}{2}-\frac{2(l_1+l_2)}{c}\right]\right\}. \tag{32}$$

3.4.2 *Signal and noise under pulsed laser illumination*

Considering the time sequence of the laser range-gated imaging system and the discrete nature of the detector unit, the illuminance on the detector unit (i, j) caused by the target and background within a pulse period can be calculated as

$$Q_u(i,j)=ab\cdot E_{su}\cdot\int_{t_d}^{t_d+t_g}\operatorname{rect}\left\{\frac{1}{t_p}\left[t+\frac{t_p}{2}-\frac{2(l_1+l_2)}{c}\right]\right\}\mathrm{d}t, \tag{33}$$

where a and b are the length and width of the detector unit, respectively.

The illuminance on the detector unit (i, j) caused by scattering of the intermediary reflective surface can be expressed, respectively, as

$$Q_{\text{back}}(i,j) = \iint_{ds} E_{\text{back}}[(i+1/2)a,(j+1/2)b]\mathrm{d}x'\mathrm{d}y' \times \int_{t_d}^{t_d+t_g} \text{rect}\left[\frac{1}{t_p}\left(t+\frac{t_p}{2}-\frac{2l_1}{c}\right)\right]\mathrm{d}t, \quad (34)$$

$$Q_d(i,j) = \iint_{ds} E_d[(i+1/2)a,(j+1/2)b]\mathrm{d}x'\mathrm{d}y' \cdot \int_{t_d}^{t_d+t_g} \text{rect}\left\{\frac{1}{t_p}\left[t+\frac{t_p}{2}-\frac{2(l_1+l_2)}{c}\right]\right\}\mathrm{d}t. \quad (35)$$

We simplify the imaging system noise and environmental noise by combining them into an equivalent incident illuminance E_{eq}, which is used as shown in the following equation:

$$Q_{\text{eq}}(i,j) = E_{\text{eq}} \cdot a \cdot b \cdot t_g. \quad (36)$$

The total disturbance of the non-line-of-sight imaging system can be expressed as

$$Q_n = Q_{\text{eq}} + Q_d + Q_{\text{back}}. \quad (37)$$

3.4.3 *Apparent contrast of the image on a photosensitive surface*

The apparent contrast of the image on a photosensitive surface can be described by

$$C(i,j,l_1,l_2) = \left|\frac{(Q_t+Q_n)-(Q_b+Q_n)}{Q_t+Q_b+2Q_n}\right| = \left|\frac{\rho_t-\rho_b}{\rho_t+\rho_b}\right| \cdot \left|\frac{1}{1+Q_n/Q_{tb}}\right| = C_0(i,j)T_{sh}(i,j,l_1,l_2), \quad (38)$$

$$Q_{tb}(l_1,l_2) = [Q_t(l_1,l_2)+Q_b(l_1,l_2)]/2, \quad (39)$$

$$T_{sh}(i,j,l_1,l_2) = \left|\frac{1}{1+Q_n/Q_{tb}}\right| < 1, \quad (40)$$

where $Q_{tb}\ (l_1,l_2)$ denotes the averaged signal of the target and background, $C_0(i,j)$ denotes the inherent contrast ratio, and $T_{sh}(i,j,l_1,l_2)$ is the contrast transfer function.

3.4.4 *Analysis and discussion*

In addition to systematic noise, the scattered disturbance illuminance from the intermediary reflective surface is the main factor in image quality degradation.

1. For photoelectric imaging systems based on human eyes, detection and identification of the extended source target depend on the target contour brought out by the apparent contrast of the image. Although people simply believe that 3 to 5% is the contrast threshold for target detection with human eyes, the more effective approaches are based on minimum resolvable contrast (MRC)[8,9] or target task performance (TTP).[10] Enhancing the apparent contrast of the image is conducive to improving the performance of non-line-of-sight imaging system.
2. It is impossible to separate $E_d(t)$ from $E_{st}(t)$ because they are synchronized with each other. However, E_{back} may be reduced or eliminated by time gating, as shown in Fig. 7.

- $l_2 \geq c \cdot t_p/2$: E_{back} is separable from $E_{st}(t)$ [as in Fig. 7(a)]. E_{back} may be filtered out completely without reducing the laser illuminance efficiency, and thus, the highest contrast image is obtained.
- $l_2 < c \cdot t_p/2$: When the gate opens upon the return of the target signal, part of the first-order backscattering is accepted by the detector, and the image contrast is decreased to some extent. To this end, the image contrast can be improved by adjusting t_d [as in Fig. 7(b)].

E_{back} can be totally filtered out by setting the strobe gating delay time to $t_d = 2l_2/c + t_p$. An optimum contrast image can be obtained if the gate width is simultaneously reduced to $t_g = 2l_2/c$. However, utilization rate of the laser illuminance decreases with increase of t_d. The laser range-gated imaging system cannot receive the target signal illuminance with $t_d = 2(l_1+l_2)/c + t_p$, and the efficiency decreases to 0. Since the laser range-gated imaging itself is low-signal-to-noise ratio (SNR) imaging, sacrificing the laser illuminance efficiency significantly reduces the SNR of the image. Therefore, practical application of non-line-of-sight imaging with laser range-gated imaging requires careful balance of the overall system.

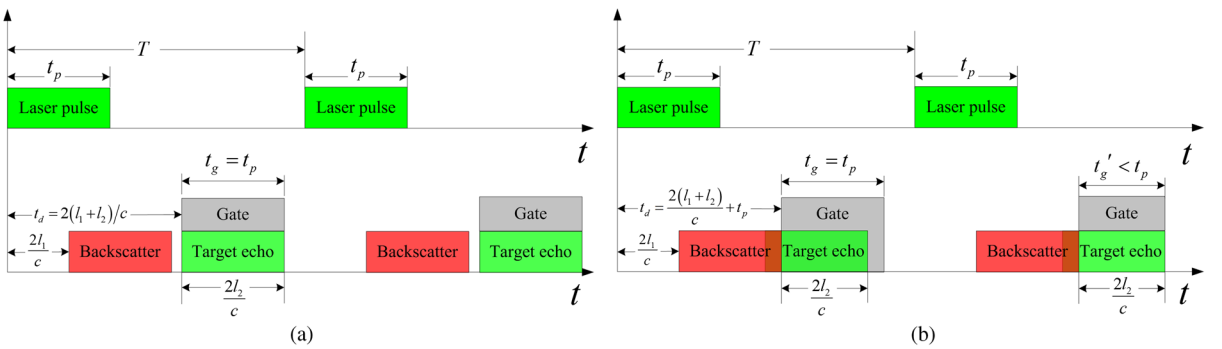

Fig. 7 Temporal relationship between pulse propagation and gated detection. (a), (b)

4 Imaging Characteristic Analysis of Non-Line-of-Sight Imaging

Based on the image contrast model of non-line-of-sight imaging constructed above, this section analyzes the non-line-of-sight imaging results with different intermediary reflective surfaces. Typical parameters of non-line-of-sight imaging with a laser range-gated imaging system are shown in Table 1. The imaging depth of field is 36 m with a laser pulse width of 120 ns and a gate width of 120 ns; 40 laser pulses are received by the photodetector within a frame when the imaging frame rate is 25 fps and the laser pulse frequency is 1000 Hz, so that a laser illuminance equivalent to 4.8 μJ is received by the photodetector per frame.

4.1 *Impacts of Reflection Characteristics of the Intermediary Reflective Surface on Non-Line-of-Sight Imaging*

The impacts of the reflection characteristics of the intermediary reflective surface on non-line-of-sight imaging are considered with $l_1 = 5$ m, $l_2 = 20$ m, and $\alpha = 45$ deg. Since $l_2 \geq c \cdot t_p/2 = 18$ m, the target signal illuminance and first-order backscattering are separable.

Figure 8 shows the curves of the target signal illuminance E_{st}, the first-order backscattering E_{back}, and the third-order forward-scattering E_d for different values of the diffuse reflectivity ρ_d of the intermediary reflective surface with a CW laser. Since E_{back} and E_d are unevenly distributed over the imaging field, the E_{back} and E_d in Fig. 8 are the respective means of E_{back} and E_d in the center area of the imaging field. The curves in Fig. 8 indicate the following conclusions:

1. Under a CW laser, the target signal illuminance E_{st} monotonically decreases with ρ_d, and first-order backscattering E_{back} monotonically increases with ρ_d. E_{st} is larger than E_{back} only when ρ_d is <0.05 (i.e., diffuse reflection takes up only 5% of the total reflection illuminance, and the specular reflection illuminance dominates), that is to say that non-line-of-sight imaging can be realized with only a CW laser when the intermediary reflective surface has very strong specular reflection characteristics. This conclusion indicates that practical realization of non-line-of-sight imaging must use a pulsed laser range-gated imaging mode in order to filter out E_{back}. In the instance indicated in Fig. 8, E_{back} can be totally filtered out without reducing the laser illuminance efficiency.
2. The target signal illuminance E_{st} spans more than three orders of magnitude from 4.6×10^{-3} W/m^2 for a completely specular reflection ($\rho_d = 0$) to 5.1×10^{-7} W/m^2 for a nearly completely diffuse reflection ($\rho_d = 0.99$). E_d is several orders of magnitude smaller than E_{st}, and E_d is two orders of magnitude smaller than E_{st} even when ρ_d is equal to 0.99. Figure 9 shows that the distribution of E_d on the photodetector for $l_1 = 5$ m, $l_2 = 20$ m, $\varphi = 0$ deg, $\theta = 2$ deg, and $\rho_d = 0.5$ is within the same order of magnitude for α (the tilt angle of the intermediary reflective surface) equals 20 or 60 deg. The image quality is severely disturbed by quantum noise when the target signal illuminance is too low, so $\rho_d \leq 0.7$ is selected as an effective non-line-of-sight imaging condition. E_{st} with $\rho_d = 0.7$ is one order of magnitude smaller than E_{st} with $\rho_d = 0$. E_d is always two orders of magnitude smaller than E_{st} when ρ_d changes from 0 to 0.7. In view of the above discussion, E_d is often negligible.

Table 1 Parameters of non-line-of-sight imaging with the laser range-gated imaging system.

Parameter	Value
ρ_t (target reflectivity)	1
ρ_b (background reflectivity)	0
Φ (energy of a single pulse in μJ)	0.12
t_p (laser pulse width in ns)	120
Laser pulse frequency in Hz	1,000
θ (divergence angle of the laser beam)	2 deg
D_0 (diameter of objective lens in mm)	20
f' (focal length of objective lens in mm)	80
τ_0 (lens transmittance)	0.9
Size of photodetector (mm^2)	14×10.5
t_g (gate width in ns)	120
Image frame rate (Hz)	25

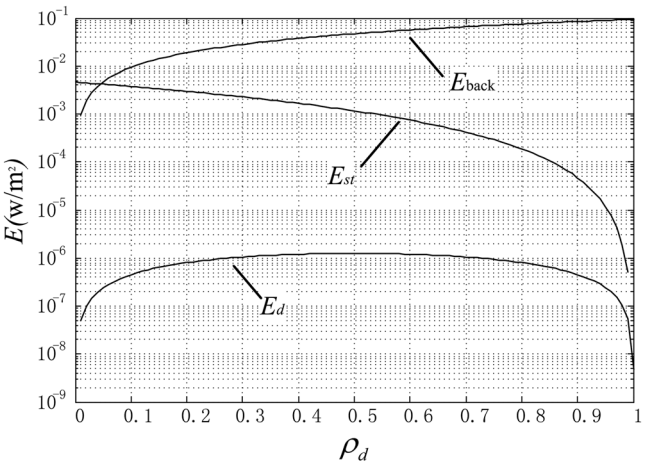

Fig. 8 Illuminance on the photosensitive surface versus ρ_d.

4.2 *Impacts of the Location of the Intermediary Reflective Surface and the Gate Width on Non-Line-of-Sight Imaging*

The parameter t_g is chosen to be equal to t_p to fully use the laser illuminance and to reduce the noise for a typical laser range-gated imaging system, in which case the imaging depth of field is $c \cdot t_p$. The gate opens when the echo signal reaches the detector, so that the gate delay time t_d equals $2(l_1 + l_2)/c$. The following discussion is based on the assumption that Q_{eq} is equal to 0.

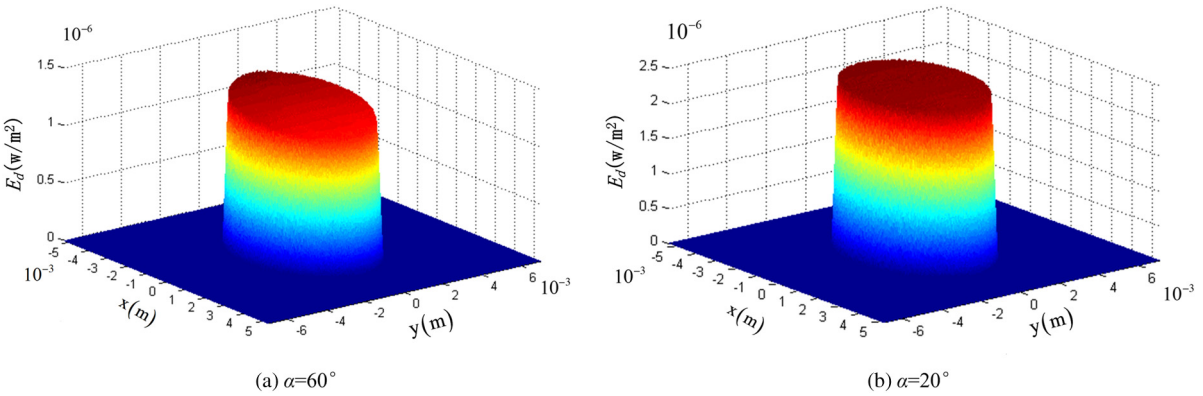

Fig. 9 Distribution of E_d on a photosensitive surface ($\varphi = 0$ deg, $\theta = 2$ deg, and $\rho_d = 0.5$). (a) $\alpha = 20$ deg, (b) $\alpha = 60$ deg.

Figure 10 shows a plot of the image contrast C versus distance l_2 with $l_1 = 5$ m and $t_d = 2(l_1 + l_2)/c$. The plot shows that C first decreases with l_2 and then increases with l_2 to a certain constant value at $l_2 = 18$ m when E_{back} is totally separated from E_{st} and that finally C is nearly fixed with increasing l_2. Figure 11 shows a plot of the image contrast C versus distance t_d with $l_1 = 5$ m and $l_2 = 10$ m. The plot shows that C increases with t_d and that C obtains its maximum value when E_{back} is totally filtered out at $t_d = 140$ ns.

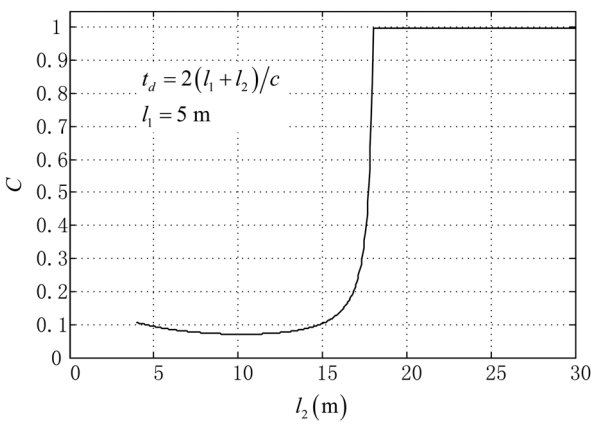

Fig. 10 C versus l_2 [$l_1 = 5$ m, $t_d = 2(l_1 + l_2)/c$].

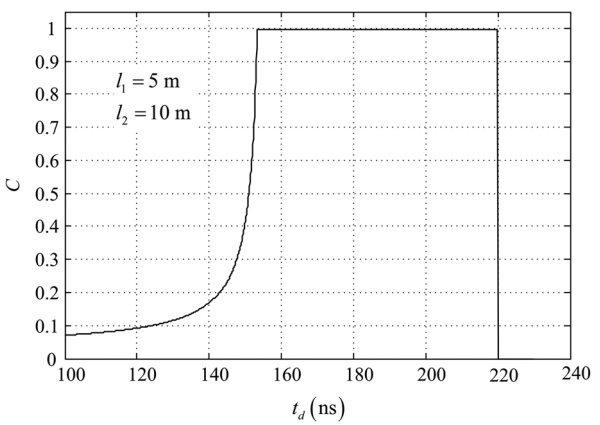

Fig. 11 C versus l_2 ($l_1 = 5$ m, $l_2 = 10$ m).

5 Conclusions

This paper describes the construction of an image contrast model of non-line-of-sight imaging with a laser range-gated imaging system on the basis of the modeling of an intermediary reflective surface. The image contrast model analyzes three factors affecting the image contrast of non-line-of-sight imaging with different intermediary reflective surfaces, where the three factors are target signal illuminance, first-order backscattering, and third-order forward-scattering. A non-line-of-sight imaging experiment simulation was carried out with the parameters of an actual laser range-gated imaging system. The simulation results show that (1) the first-order backscattering is the dominant disturbance to non-line-of-sight images and can be effectively filtered out by laser range-gated imaging and (2) the effect of the third-order forward-scattering on non-line-of-sight images is often negligible since the third-order forward-scattering is insignificant compared to the target signal illuminance in most cases. The image contrast model of non-line-of-sight imaging with a laser range-gated imaging system gives insights into the theoretical analysis and system design of non-line-of-sight imaging.

The simulation results also show that the reflection characteristics of the intermediary reflective surface have a significant effect on non-line-of-sight imaging. The bidirectional reflectance distribution function (BRDF) is a more comprehensive description of surface reflection characteristics; thus, BRDF modeling of typical construction material surfaces is a direction for further research. Meanwhile, since non-line-of-sight imaging with laser range-gated imaging system is usually low-SNR imaging, estimating the range of non-line-of-sight imaging using MRC or TTP is another direction for further research.

Acknowledgments

This work was supported by the Specialized Research Fund for the Doctoral Program of Higher Education (No. 20111101110013) and the Foundation of the Science and Technology on Low-Light-Level Night Vision Laboratory (No. J20110504). The authors would like to thank all the reviewers for their helpful comments and constructive suggestions. They would also like to thank Mr. Ye Peng and Dr. Xuan Hongwen for their assistance with the programming.

References

1. E. Repasi et al., "Mono- and bi-static SWIR range-gated imaging experiments for ground applications," *Proc. SPIE* **7114**, 71140D (2008).
2. E. Repasi et al., "Advanced short-wavelength infrared range-gated imaging for ground applications in monostatic and bistatic configurations," *Appl. Opt.* **48**(31), 5956–5969 (2009).
3. O. Steinvall, M. Elmqvist, and H. Larsson, "See around the corner using active imaging," *Proc. SPIE* **8186**, 818605 (2011).
4. A. Kirmani et al., "Looking around the corner using transient imaging," in *IEEE 12th Int. Conf. on Computer Vision*, pp. 159–166, Springer, Netherlands (2009).
5. O. Gupta et al., "Reconstruction of hidden 3D shapes using diffuse reflections," *Opt. Express* **20**(17), 19096–19108 (2012).
6. X. Kai-da et al., "Survey on technical development and combined application mode of laser range-gated imaging system," *Infrared Technol.* **34**(1), 16–23 (2012).
7. X. Kaida et al., "Non-line-of-sight imaging based on laser range-gated imaging technology," *Infrared Laser Eng.* **41**(8), 2073–2078 (2012).
8. J. Wei-qi et al., "A model to predict range performance of imaging system for extended target based on minimum resolvable contrast," *Acta Optica Sinica* **29**(6), 1552–1556 (2009).
9. G. Arthur, "Prediction and measurement of minimum resolvable contrast for TV sensors," *Proc. SPIE* **2223**, 533–542 (1994).
10. R. H. Vollmerhausen et al., "New metric for predicting target acquisition performance," *Opt. Eng.* **43**(11), 2806–2818 (2004).

Kaida Xu received his BS from Mechanical Engineering College, China, in 2001. He is currently pursuing his PhD in optical engineering at Beijing Institute of Technology, China. His technical interests include low-level-light and infrared imaging technology.

Weiqi Jin received his PhD in optical engineering from Beijing Institute of Technology of China in 1990. He is currently a professor with the Department of Optical Engineering in the School of Optoelectronics at the Beijing Institute of Technology. His major research interests include low-level-light imaging, thermal imaging, and image processing. He is a fellow of SPIE.

Shenyou Zhao received his BS in control technology and instrument from Changchun University of Science and Technology in 2011. He is currently pursuing his master's degree in optical engineering at Beijing Institute of Technology, China. His main technical interest is optical imaging technique.

Jing Liu received her BS in optical engineering from Beijing Institute of Technology of China in 2009. She studied augmented reality in Universidad Politecnica de Madrid of Spain from March to September 2009. She is currently pursuing her PhD in optical engineering at Beijing Institute of Technology of China. Her technical interests include underwater imaging, laser range-gated imaging, polarization imaging, and imaging process.

Hui Guo received her PhD in optical engineering from Beijing Institute of Technology in 2005. She is currently a doctoral supervisor in the National Key Laboratory of Science and Technology on Low Light Level Night Vision, Xi'an, China. Her major research direction is low-light-level night vision technology.

Su Qiu received his PhD from School of Optoelectronics at Beijing Institute of Technology in 2013. He is currently an assistant professor in School of Optoelectronics at Beijing Institute of Technology. His major research interests include digital image processing, low-level-light and infrared imaging technology.

Dongsheng Wu obtained his master's degree in optical engineering from Mechanical Engineering College in 2003 and engaged in the work of photoelectric detection and tracking.